nature communications

Article

https://doi.org/10.1038/s41467-025-63316-2

A quadratic paradigm describes the relationship between phenotype severity and variation

Received: 20 March 2025

Accepted: 15 August 2025

Published online: 01 September 2025

Check for updates

Abigail Mumme-Monheit[1], Grace E. Gustafson[1], Colette A. Hopkins[1], Raisa Bailon-Zambrano[1], Juliana Sucharov[1], Michael J. Lippincott[2], Gregory P. Way[2], Kathryn L. Colborn[3] & James T. Nichols[1]

In 1942 Waddington observed that phenotype variation among mutant animals is greater than in wild types. Here we update this observation to depict unexpected relationships between phenotype severity and variation. Using a zebrafish *mef2ca* allelic series representing a range in craniofacial phenotype severity, we tested the straightforward hypothesis that as phenotype severity increases, variation increases. We found that severity and variation were positively correlated, but only to a point. Variation collapsed in the most severe conditions. Mathematically, we found that the best fit for the relationship between severity and variation is a quadratic function. Across both zebrafish craniofacial phenotypes and human genetic disease, wild-type conditions produced low variation, moderate severity was associated with high variation, and conditions of extreme severity resulted in low variation. We propose that the quadratic relationship between severity and variation is a universal principle of biology that until now has not been formally tested.

It has long been observed that variation among mutant organisms is greater than the variation in wild types[1]. These observations were foundational in Waddington's now-famous canalization metaphor, where he visualized development as a ball rolling down a hill, with canals maintaining the developmental trajectory. Waddington's canals described the buffering of development against environmental or genetic perturbations, or the tendency to arrive at a specific phenotype. As such, in canalized systems, developmental outcomes display increased robustness to perturbation, resulting in reduced phenotype variation[2–4]. Conversely, a phenomenon known as decanalization, or loss of robustness, in mutant genotypes results in more variable mutant phenotypes compared with wild types. Mutant decanalization appears to be a broadly generalizable biological phenomenon[1]. However, whether the amount of mutant variation correlates with the severity of the mutant phenotype has not yet been explicitly addressed. Severity can be best understood by both phenotype penetrance and expressivity. In this study, we define penetrance as the frequency of a phenotype that is associated with a genotype[5], and expressivity as the magnitude of difference from the wild-type phenotype. Moreover, we find here that expressivity and penetrance are strongly correlated. We primarily use expressivity as a continuous measure of severity to understand the relationship between severity and variation. It seems reasonable to predict a linear relationship where more severe mutants produce more variation while less severe mutants produce less variation, but this has not yet been formally examined. Here, we seek to answer the question: Are severity and variation positively correlated?

Mechanisms underlying phenotypic variation have been explored with numerous systems. Stochastic transcriptional noise, variable paralogous compensation, and molecular chaperones are all established factors contributing to developmental robustness, or loss of robustness in mutants[5–10]. Surprisingly, the precise relationship between mutant severity and variation has not yet been delineated for any of these mechanisms. How variation correlates with gene dosage was partially explored via quantitative phenotyping of an *Fgf8* allelic

[1]Department of Craniofacial Biology, University of Colorado Anschutz Medical Campus, Aurora, CO, USA. [2]Department of Biomedical Informatics, University of Colorado Anschutz Medical Campus, Aurora, CO, USA. [3]Department of Surgery, University of Colorado Anschutz Medical Campus, Aurora, CO, USA. e-mail: james.nichols@cuanschutz.edu

series in mice[11]. This study showed that a partial decrease in *Fgf8* dose produced low craniofacial variation, while lowering *Fgf8* dosage below a threshold produced higher craniofacial phenotype variation, illustrating a nonlinear relationship between gene dosage and phenotype. However, these authors did not test if phenotype variation is positively correlated with phenotype severity, which we do here. Moreover, the genotypes with the lowest *Fgf8* dosage could not be included in this study due to early lethality. Thus, this *Fgf8* allelic series motivates careful examination of the relationship between phenotype severity and variation, which remains incompletely understood.

The observation that phenotypes are more variable in mutant conditions has been described in both model organisms and human genetic disorders[12–14]. Variable and incompletely penetrant craniofacial phenotypes are observed in patients with *MEF2C* haploinsufficiency syndrome, a disorder caused by different de novo mutations in the *MEF2C* transcription factor encoding gene[15–17]. One barrier to studying mutant phenotype variation in these humans is that the same allele cannot be studied across many individuals. When this disorder is modeled in zebrafish by mutating the *MEF2C* ortholog, *mef2ca*, variations in phenotype severity and penetrance are also observed, providing a model to study variation within a given mutant allele[5,18–20]. A strength of this zebrafish system is the ability to generate numerous different mutant alleles that produce a different average phenotype severity. Moreover, large numbers of mutants can be easily obtained, powering rigorous study of both among- and within-individual variation[5]. Among-individual variation is measured by calculating the variance of a trait within a population. Within-individual variation can be measured by calculating asymmetry, or deviations from anticipated bilateral symmetry. There are different types of asymmetries in developmental systems[21]. Fluctuating asymmetry is the random, normally distributed variation of the difference between left and right[22]. Another type is directional asymmetry, where the same side is consistently larger than the other[23]. Fluctuating asymmetry is often used as a readout of developmental stability, or the tendency of traits to resist the effects of developmental noise given an organism's genotype and particular environment[24]. However, estimating developmental stability using fluctuating asymmetry requires, at a minimum, the removal of directional asymmetry[22,23,25–28], and systems with significant directional asymmetry are better excluded altogether from studies wishing to examine fluctuating asymmetry[26]. Both directional and fluctuating asymmetry have been previously observed in our system[5,18,29]. Thus, we do not address developmental stability in this study. Rather, we use both absolute differences between left and right, which we call absolute asymmetry, and directional asymmetry as measures of within-individual variation. Nevertheless, the zebrafish *mef2ca* mutant model provides a highly refined system in which to study the relationship between severity and both among- and within-individual variation.

Unique to this study, we achieve great granularity in phenotype severity levels across biological systems in order to uncover a generalizable relationship between severity and variation. We hypothesized that as severity increased, variation would increase. First, we studied homozygous and heterozygous conditions of three *mef2ca* mutant alleles to study differences in penetrance and expressivity. We introduce a new allele, which is a full deletion of the *mef2ca* locus. Interestingly, we observe that despite being null for *mef2ca*, this allele does not represent the most severe condition. We previously demonstrated that other *mef2* paralogs are partially redundant with *mef2ca* in zebrafish craniofacial development[5]. Thus, this deletion allele does not represent full loss of *mef2* function. To modulate severity, we combined each of the *mef2ca* alleles with a decanalizing transgene that, as we previously demonstrated for a different locus, increases phenotype penetrance[30]. Combining these genomic features allowed us to generate 18 genotypes, for which we could evaluate penetrance. We next measured a single linear craniofacial element in all genotypes to quantify severity, among-individual variation, and within-individual variation. By plotting variance against severity, we were able to demonstrate that there is an unexpected quadratic relationship between variation and severity. We also demonstrated that other zebrafish phenotypes exhibit a collapse in variation in high-severity conditions. Further, we found that this relationship is generalizable to a human disease phenotype, age of Huntington's disease onset. Our findings further our understanding of canalization, demonstrating how wild-type canalized systems become decanalized in mid-severity mutants, then an invariant phenotype becomes fixed in the most severe mutant conditions, which we call neocanalization.

Results

A *mef2ca* allelic series reveals differences in severity and variation

We examined three different, individually identified and generated *mef2ca* mutant alleles (Fig. 1a). The *mef2ca*^{b1086} and *mef2ca*^{b631} alleles were identified in ENU mutagenesis screens and have been examined in multiple studies[5,18–20,29]. These alleles contain point mutations causing an early stop codon and a mutation in the start codon, respectively (Fig. 1a). We also generated a new allele, *mef2ca*^{co3008}, containing a large deletion encompassing the entire coding region.

Homozygous mutants for all of these lesions show incomplete penetrance and variable expressivity of craniofacial skeletal phenotypes observed by staining bone and cartilage (Fig. 1b). Mutant-associated phenotypes never appear in wild-type siblings. Penetrance of these phenotypes is lower in the *mef2ca*^{b631} allele compared to both the *mef2ca*^{co3008} and the *mef2ca*^{b1086} alleles (Supplementary Table 1). A specific phenotype associated with *mef2ca* mutation, a shortened symplectic region of the hyosymplectic cartilage (referred to as symplectic cartilage), allows for precise quantitative characterization of expressivity in different mutant alleles and conditions[5] (Fig. 1c). We found that the length of this cartilage is strongly correlated with overall penetrance of mutant phenotypes (Supplementary Fig. 1). Thus, symplectic cartilage length is an appropriate proxy for mutant phenotype severity. Using this metric, a larger magnitude of difference from the wild type indicates a more severe condition; the more severe individuals produce a shorter symplectic cartilage. The length of this cartilage provides a continuous variable that can be easily measured in many individuals. We found that the total symplectic cartilage length (left symplectic plus right symplectic length) was significantly shorter, more severe, in all mutant alleles compared with wild types (Fig. 1d). Additionally, the *mef2ca*^{co3008} and *mef2ca*^{b1086} alleles had symplectic cartilages that were significantly shorter than the *mef2ca*^{b631} allele. We can also use the spread of these symplectic cartilage lengths to look at among-individual variation. We observed that, in line with Waddington's observations, there is increased among-individual variation in all mutants compared with wild types (Supplementary Table 2). We further used absolute asymmetry (absolute difference between left and right symplectic cartilage length) to measure within-individual variation, revealing that all mutants exhibited significantly more asymmetry than wild types, but that none of the mutant alleles were significantly different from each other (Fig. 1e).

The *fli1:Gal4* transgene increases phenotype severity in every *mef2ca* allele

Gal4 transgenes have been used extensively in zebrafish, though studies acknowledge that this transgene may adversely affect development[31]. In this study, we use a *fli1:Gal4* transgene to modulate severity. Our previous work using this transgene, which drives expression of Gal4 in the cranial neural crest, demonstrated that craniofacial phenotypes in *fras1* zebrafish mutants had higher penetrance in the presence of this transgene[30]. We posited that the more severe phenotypes were due to decanalization by the transgene, so we sought to determine if this effect on penetrance would persist in other zebrafish mutants like *mef2ca*. Consistent with our previous study, when

https://doi.org/10.1038/s41467-025-63316-2

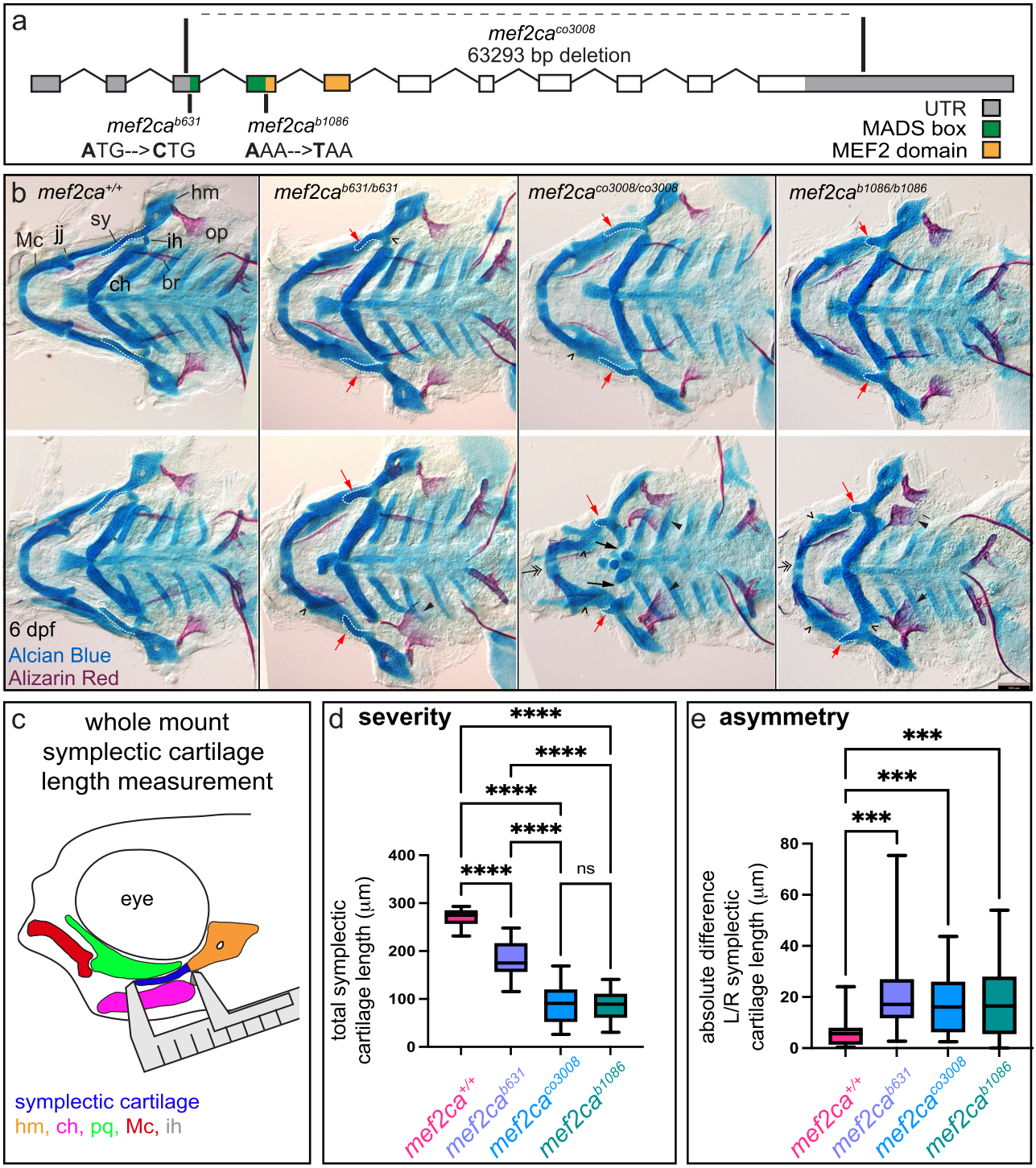

the *fli1:Gal4* transgene is present in an otherwise wild-type animal, craniofacial phenotypes are overtly indistinguishable from those of *fli1:Gal4* negative siblings (Fig. 2a). In the absence of the transgene, animals heterozygous for *mef2ca* are also indistinguishable from wild types. Examining both the quantitative and continuous symplectic cartilage length phenotype expressivity and overall phenotype penetrance, we further found that the *fli1:Gal4* transgene made severity significantly worse in homozygous mutants compared to homozygous *mef2ca* mutant non-transgenic siblings (Fig. 2b, Supplementary Fig. 2). Additionally, symplectic cartilage length was significantly shorter across all *mef2ca*-like genotypes in the presence of the transgene (Fig. 2b). All homozygous mutant symplectic cartilages were significantly shorter than wild types and heterozygotes (Supplementary Table 3). Further, in the presence of the *fli1:Gal4* transgene, *mef2ca*^{b1086} and *mef2ca*^{co3008} heterozygotes were significantly more severe than wild types and had incompletely penetrant *mef2ca* mutant-associated phenotypes (Fig. 2b, Supplementary Fig. 2).

Examining absolute asymmetry for each allele, we find that transgenic *mef2ca*^{b1086} and *mef2ca*^{co3008} heterozygotes exhibit increased within-individual variation compared to non-transgenic wild types (Fig. 2c). Without the *fli1:Gal4* transgene, within-individual variation is increased in all homozygous mutants compared with wild types. However, within-individual variation in the most severe conditions, *mef2ca* homozygous mutants in the presence of the transgene, collapsed down to wild-type levels, except for in the mildest allele, *mef2ca*^{b631}. Thus, we demonstrated that the *fli1:Gal4* transgene

Fig. 1 | A *mef2ca* allelic series demonstrates a range of severity and variation. **a** Schematic of *mef2ca* genomic structure. All *mef2ca* mutant alleles and regions encoding known functional domains are annotated. **b** Heterozygotes for each *mef2ca* allele were pairwise intercrossed, and six days post-fertilization (dpf) larvae were stained with Alcian Blue and Alizarin Red to label cartilage and bone, respectively. The individuals were then genotyped, and the viscerocranium was dissected, flat-mounted, and imaged. Two full-sibling individuals are shown for each genotype to illustrate among-individual variation. Within-individual variation can be observed by comparing the left and right sides of a given skeleton. The following craniofacial skeletal elements are indicated in a wild-type individual: opercle bone (op), branchiostegal ray (br), Meckel's (Mc), ceratohyal (ch), symplectic (sy) cartilages, interhyal (ih) and jaw (jj) joints. The symplectic cartilage is outlined with a white dashed line in all individuals. Indicated phenotypes associated with *mef2ca* mutants include: ectopic bone (arrowheads), interhyal and jaw-joint fusions (^), dysmorphic ch (arrows), reduced Mc (double arrowhead), and a shortened sy (red arrows). Scale bar is 100 μm. **c** Schematic depicting how symplectic cartilage length was measured from 6 dpf larvae. **d** Symplectic cartilage length was measured from 6 dpf larvae homozygous for the indicated *mef2ca* allele, and the left symplectic length was added to the right symplectic length to get a total length for each animal. The *p*-values from a two-sided Dunnett T3 test are indicated (****≤0.0001). **e** Symplectic cartilage length on the left and right sides of 6 dpf zebrafish was measured to determine asymmetry or the absolute difference between left and right for fish homozygous for the indicated alleles. The *p*-values from a two-sided Dunnett T3 test are indicated (***≤0.001, wild type vs. *b631* $p = 0.0002$, wild type vs. *co3008* $p = 0.0003$, wild type vs. *b1086* $p = 0.0008$). There is no significant difference in asymmetry between any of the mutant alleles. In box and whisker plots, the box covers the 25th to 75th quartiles, the line is at the median, and whiskers extend to the minimum and maximum values. The following *n* numbers represent biological replicates (individual animals) for (**d**) and (**e**): wild type 23, *b631* 28, *co3008* 30, *b1086* 34. Source data are provided as a Source Data file.

increases severity across our allelic series, providing a deep dataset to calculate the relationship between severity and variation.

A quadratic function describes the relationship between severity and variation

We then used symplectic cartilage measurements from all conditions to directly test the hypothesis that variation is positively correlated with severity. The different symplectic cartilage lengths measured for each genotype allowed us to evaluate among-individual variation and severity for each condition. We used variance to quantify variation because this statistic captures how much the values are distributed around the mean[32]. Further, variance is appropriate for this single dataset with a similar magnitude of measurement for all conditions. Each genotype was represented by a single point, where average symplectic cartilage length was plotted on the *x*-axis (severity), and variance of symplectic length was plotted on the *y*-axis. This allowed us to plot variation by severity for all genotypes and observe an overall relationship. We then used a cubic smoothing spline in an exploratory analysis to identify the relationship that best fit these data (Supplementary Fig. 3a), finding that the spline resembled a quadratic relationship. Smoothing splines are nonparametric functions that can be used to illustrate the relationship between two variables when a nonlinear trend is observed in a scatterplot. We then fit a linear model with a quadratic trend specifying length plus length squared as the linear predictor and variation as the outcome (Fig. 3a, Supplementary Table 4) to mimic the trend we saw in the smoothing spline using a parametric model. This model had an adjusted R-squared of 0.52. Compared to a linear model with a linear relationship fit between length and variance with an R-squared of 0.07, the quadratic model was a much better fit. As predicted, severity and variation were positively correlated, but only to a point. Unexpectedly, variation collapses in the more severe conditions.

We were interested in identifying whether this relationship holds true for within-individual variation, or absolute asymmetry, for the symplectic cartilage phenotype. Using the same mathematical approach, but plotting mean absolute value of left-right asymmetry on the *y*-axis against mean symplectic length on *x*-axis, we again found that the spline resembled a quadratic relationship (Supplementary Fig. 3b). We then fit a linear model with mean length plus mean length squared regressed on variance, yielding an R-squared of 0.75 (Fig. 3b). A linear fit between variance and mean length yielded an R-squared of 0.23. Hence, a quadratic model was again a better fit for the relationship between symplectic cartilage length and variation. Finally, we found that directional asymmetry also followed a similar trend (Supplementary Fig. 4). Our discovery that both among- and within-individual variation fit the quadratic model suggests that this paradigm might be more generalizable to other phenotypes within this system.

Variation in dermal bone phenotypes expands and collapses in mid- and high-severity mutants, respectively

Next, we explored whether the collapse in variation in high-severity conditions that we observed with the symplectic cartilage was also present in other parts of the craniofacial complex within the same biological system. We imaged opercle bone and branchiostegal ray complexes from larvae fluorescently stained with Alizarin Red from wild-type, mid-severity and high-severity conditions (Fig. 4a). In this experiment, we used wild-type, unselected, and selectively bred[19,20,33] *mef2ca*^{co3008} mutant strains for low, mid, and high-severity conditions, respectively. Unlike the easily measured symplectic cartilage, more complex imaging and analyses are required to study variation in these structures. While opercle-branchiostegal ray complexes were similarly shaped in wild types, there were many different shapes observed in the mid-severity mutants, as previously reported for *mef2ca* mutants[19,29]. Strikingly, when we examined these bones in high-severity conditions, all bones were again similarly shaped (Fig. 4a). Specifically, in the severe strain, all the opercle branchiostegal ray complexes were fully fused. To quantify this variation, we measured the bone area in these genotypes finding that area variance was significantly higher in the mid-severity mutants compared with both wild types and high severity when each complex, left and right sides, was treated independently (Fig. 4b). When left and right sides were summed, mid-severity mutants displayed higher variation than wild types. We found there was no difference in variation between mid- and high-severity mutants, likely due to the smaller sample size. There were no significant differences in absolute asymmetry between genotypes; however, a trend towards higher asymmetry in the mid-severity condition was observed. Previous work demonstrates that the changes in the opercle-branchiostegal ray bones associated with *mef2ca* mutation are due to changes in shape[18]. Thus, area does not fully represent the complexity of the shapes that these bones take in our wild-type and mutant conditions.

Since the varying morphologies of this bone complex across conditions make geometric morphometric analyses impossible[29], we used unbiased image-based profiling[34] to quantify the shape variation that is readily observed by eye. This automated image analysis pipeline measured hundreds of different image features from this dataset. For each individual feature, we calculated the variance within each condition (Supplementary Table 5). Each image feature belongs to one of six classes −area shape, granularity, radial distribution, intensity, neighbors, and texture. To examine variance for each of the feature classes, we generated box and whisker plots. In these plots, variances for each individual feature belonging to a given class were plotted. For each feature class, we used a Welch ANOVA and Dunnett T3 test to evaluate significant differences between mean variances for each condition: low, mid, and high severity. These analyses demonstrate that, overall, area shape feature variances fit the low-high-low variance trend in low-mid-high-severity conditions, respectively, as predicted by the quadratic relationship

https://doi.org/10.1038/s41467-025-63316-2

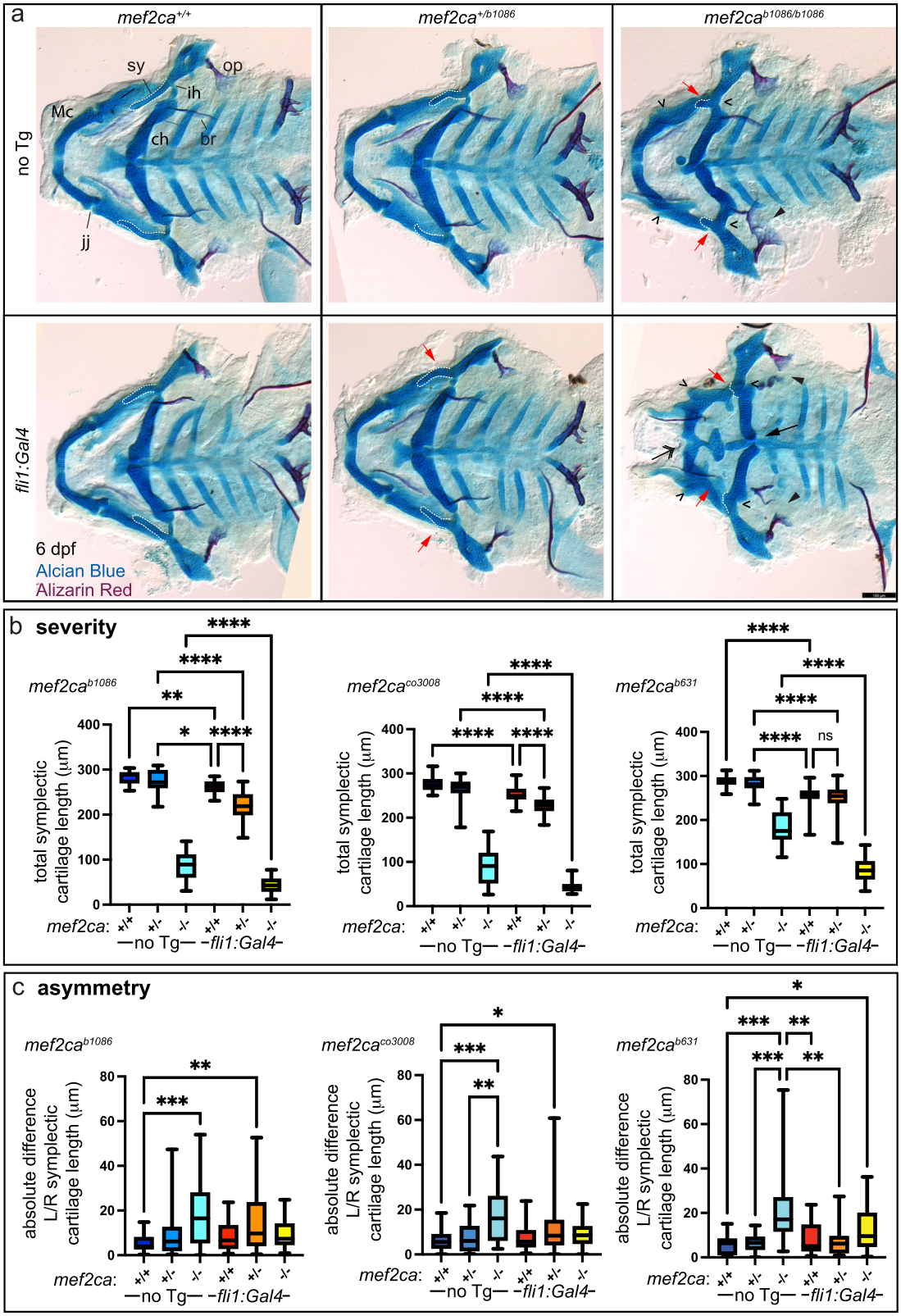

model. Importantly, the other non-area shape feature classes did not fit this trend (Supplementary Fig. 5). We further scored how many individual features within a feature class fit the expected low-high-low variance trend and calculated the frequency of this trend within each class, not considering statistical significance for each individual feature (Supplementary Table 6). These analyses demonstrate that area shape features more frequently fit the predicted trend (68% of individual area shape features) compared with other classes (for example, 21% of individual texture features). These unbiased computational approaches indicate that shape variation is low in low-severity conditions, high in mid-severity conditions, and low again in high-severity conditions. We then sought to understand whether this relationship could be extended to other biological systems with similarly tractable and measurable phenotypes beyond the zebrafish craniofacial complex.

https://doi.org/10.1038/s41467-025-63316-2

Fig. 2 | A decanalizing transgene increases *mef2ca* mutant phenotype severity. **a** Zebrafish double heterozygous for the *mef2ca*^{b1086} allele and the *fli1:Gal4* transgene were outcrossed to zebrafish heterozygous for the *mef2ca*^{b1086} allele. Larvae were fixed and stained with Alcian Blue and Alizarin Red at six dpf, genotyped, and the viscerocranium was dissected and flat-mounted. The following structures are labeled in the *fli1:Gal4* negative wild type: opercle bone (op), branchiostegal ray (br), symplectic (sy), ceratohyal (ch), and Meckel's (Mc) cartilages. The symplectic cartilage is outlined with a white dashed line in all individuals. Phenotypes associated with *mef2ca* mutations are indicated as follows: ectopic opercle bone (arrowhead), shortened symplectic (red arrow), dysmorphic ceratohyal (arrow), reduced Meckel's cartilage (double arrowhead), interhyal and jaw-joint fusions (^). Scale bar is 100 µm. **b** Total symplectic cartilage length was measured in six dpf larvae for all *mef2ca* mutant alleles, then plotted by *mef2ca* genotype and presence or absence of the *fli1:Gal4* transgene. Asterisks indicate significant differences in symplectic cartilage length between genotypes. The *p*-values from a two-sided Dunnett T3 test are indicated (*≤0.05, **≤0.01, ***≤0.001, ****≤0.0001). Some significance indications are omitted for clarity, for example, all homozygous mutants were significantly different from all wild types and all heterozygotes (*p*-value < 0.0001). For all *p*-values comparing all conditions, see Supplementary Table 3. **c** Symplectic cartilage length on the left and right sides of 6 dpf zebrafish was measured to determine asymmetry or the absolute difference between left and right. The left-right asymmetry is plotted by *mef2ca* genotype and presence or absence of the *fli1:Gal4* transgene. The *p*-values from a two-sided Dunnett T3 test are indicated (*≤0.05, **≤0.01, ***≤0.001, ****≤0.0001, exact *p*-values are presented in Supplementary Table 3). In box and whisker plots, the box covers the 25th to 75th quartiles, the line is at the median, and whiskers extend to the minimum and maximum values. The following *n* numbers represent biological replicates (individual animals) for (**b**) and (**c**): *b1086*; +/+Tg- 15, +/-Tg- 34, -/-Tg- 34, +/+Tg+ 28, +/-Tg+ 44, -/-Tg+ 28. *co3008*; +/+Tg- 29, +/-Tg- 41, -/-Tg- 30, +/+Tg+ 25, +/-Tg+ 49, -/-Tg+ 32. *b631*; +/+Tg- 25, +/-Tg- 30, -/-Tg- 28, +/+Tg+ 31, +/-Tg+ 30, -/-Tg+ 24. Source data are provided as a Source Data file.

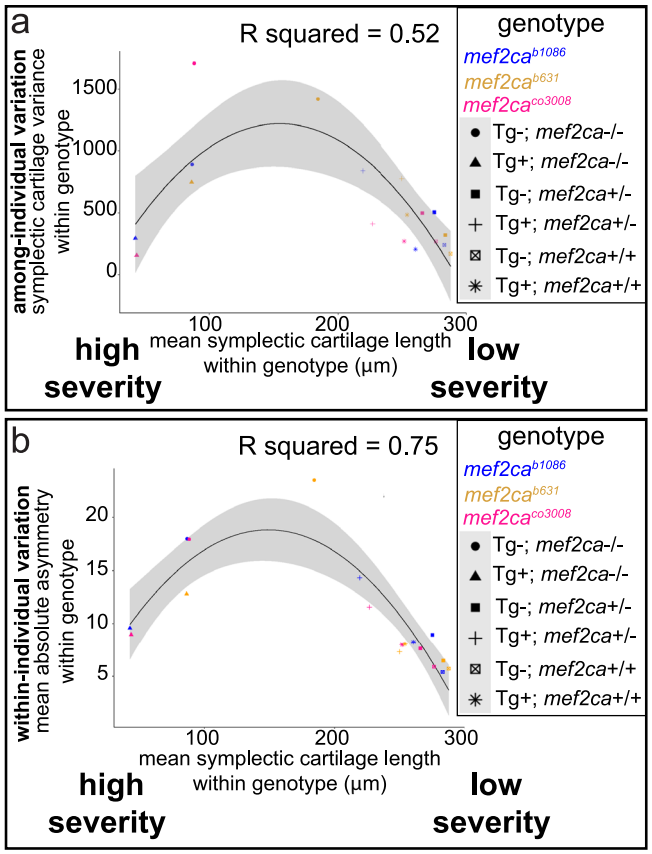

Fig. 3 | The relationship between phenotype severity and variation fits a quadratic trend. **a** Each genotype was plotted as a single point determined by the mean symplectic length and variance, representing among-individual variation, for that genotype. Alleles are indicated by color, and genotypes are indicated by shape for each point. The R-squared for the quadratic equation that represents the relationship between among-individual variation and severity is indicated. **b** Each genotype was plotted by the average left/right asymmetry, representing within-individual variation, against mean symplectic length. The R-squared for the quadratic equation that represents the relationship between within-individual variation and severity is indicated. The gray bands in (**a**) and (**b**) represent 95% confidence intervals. Source data are provided as a Source Data file.

Huntington's disease onset follows the quadratic trend

Finally, we looked to test this relationship in a human disease model, specifically Huntington's disease. There is a well-documented association between higher number of CAG repeats and earlier age of symptom onset in patients with Huntington's disease[35,36], which we interpret as more severe disease. Huntington's disease is well-suited to test our phenotypic variation and severity hypothesis, as individuals with different numbers of repeats generate an allelic series with many individuals within each class or genotype. Further, age of onset is a continuous variable with a range of severity (Fig. 5a). Similar to our zebrafish data, we first used a smoothing spline to visualize the relationship between severity and variation (Supplementary Fig. 6). This resembled a quadratic, which we found had an adjusted R-squared of 0.14 (Fig. 5b). Compared to a linear model with a linear relationship fit between length and variance with an R-squared of 0.05, the quadratic model was a much better fit. We observed that there were some potential outliers in these data that might be driving this fit. To test this, we omitted genotypes with variances greater than 600 and found that this increased the R-squared for the quadratic fit to 0.33, indicating that the quadratic fit was not driven by the outliers (Fig. 5c).

Discussion

Our zebrafish system is well-suited to formally test the relationship between phenotype severity and variation. Unexpectedly, we found that this relationship is best fit by a quadratic model. Employing a range of techniques across systems validated this relationship, indicating it may be a fundamental biological phenomenon. We demonstrate that the same relationship holds true in craniofacial phenotypes in zebrafish and Huntington's disease phenotypes in humans. We predict that more examples of this phenomenon will emerge from other systems. However, a suitable system must include numerous alleles, with numerous observations for each allele, and a continuous phenotype, like symplectic cartilage length in *mef2ca* mutants. By combining what we have learned from these models, we can develop a new paradigm extending the relationship that Waddington first identified. By looking beyond a dichotomous comparison between mutants and wild types, we empirically demonstrated that as phenotypic severity moves away from the wild type, variation first increases, but then decreases in the maximally affected conditions.

Previous work has differentiated between canalization and developmental stability as arising from different biological mechanisms[4]. Specifically, canalization minimizes the impact of environmental and genetic variation, whereas developmental stability occurs in the same genotype in the same organism and is thought to buffer stochastic variation[24]. We are not able to measure developmental instability, as determined by fluctuating asymmetry, due to the prevalent directional asymmetry in our system. However, we use asymmetries in general to observe that within-individual variation follows the same quadratic trend as among-individual variation. Thus, we propose that asymmetries, independent of directional versus fluctuating, can be used as a measurement of canalization. Traits can be canalized to left-right invariance, left-right asymmetry can arise during decanalization, and traits are again canalized to left-right invariance in severe conditions, as we observed in our system. This finding suggests that the quadratic relationship between severity and variation holds true irrespective of the type of variation.

https://doi.org/10.1038/s41467-025-63316-2

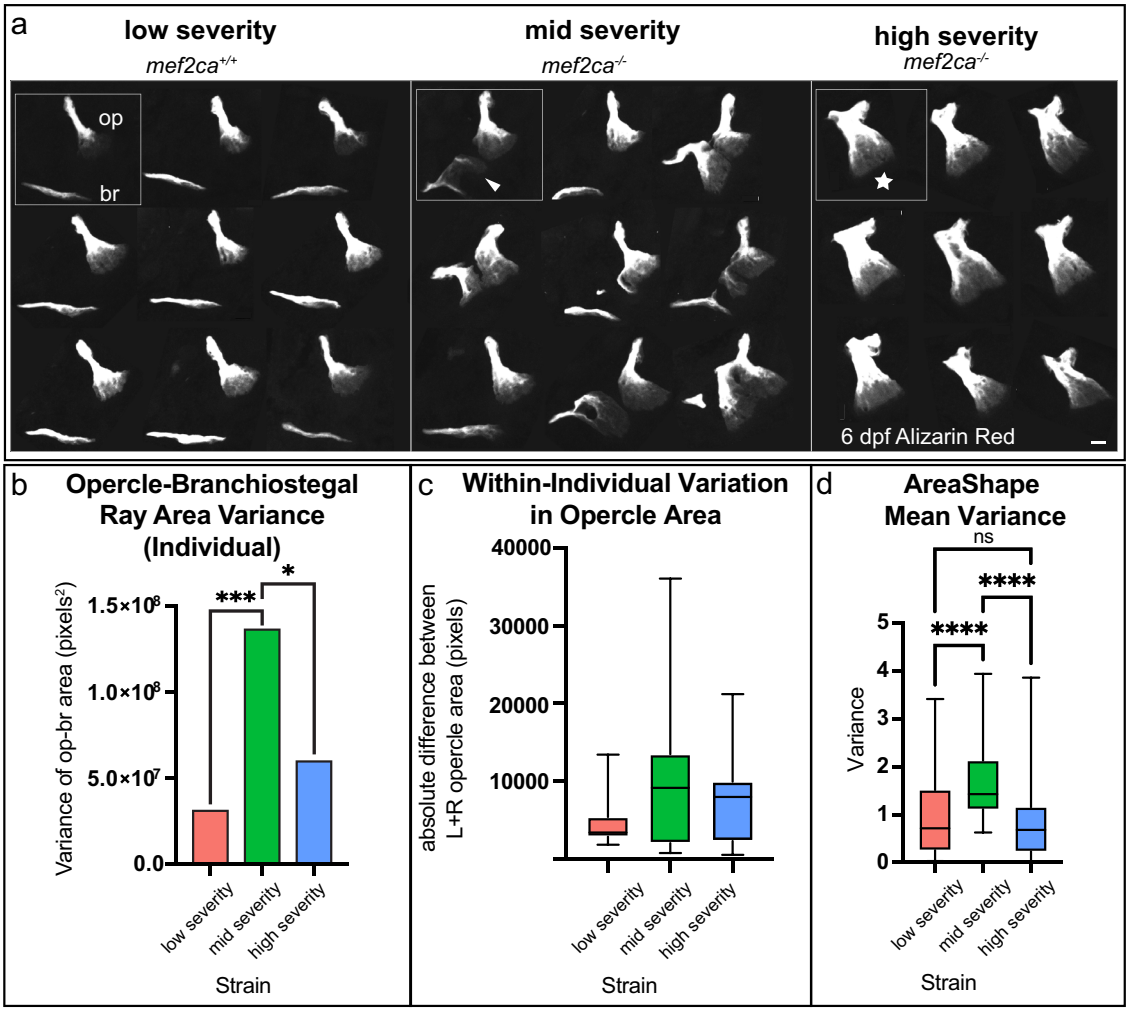

Fig. 4 | The relationship between phenotype variation and severity can be observed in opercle-branchiostegal ray (op-br) complexes. a Nine op-br complexes are shown for each genotype. Three severity classes are shown—low severity (wild types), mid severity (unselected homozygous *mef2ca*^{ca3008} mutants), and high severity (selectively bred high-penetrance homozygous *mef2ca*^{ca3008} mutants[19,20,33]). These animals were stained with Alizarin Red at 6dpf and imaged by whole-mount confocal microscopy. **b** Variance of op-br complex area was calculated for each severity class. Area variance was calculated among all op-br complexes imaged. A two-sided F-test was used to test equality of variances, and *p*-values are indicated (*≤0.05 $p = 0.039$, ***≤0.001 $p = 0.0003$). **c** Within-individual variation was also plotted by taking the absolute value of the difference in area between left and right op-br complexes. **d** Variances were calculated for all area shape features and plotted on a box and whisker plot. Average variance is higher in the mid-severity strain than in the other two strains. The *p*-values from a Dunnett T3 test are indicated (****≤0.0001). For (**c**) and (**d**) box and whisker plots, the box covers the 25th to 75th quartiles, the line is at the median, and whiskers extend to the minimum and maximum values. Source data are provided as a Source Data file.

Separate from our central findings on the relationship between phenotype severity and variation, we find support for the observation that the *fli1:Gal4* transgene has destabilizing effects on zebrafish craniofacial mutants. The worsening of mutant phenotypes in the presence of the *fli1:Gal4* transgene provides an interesting avenue for future investigation into the mechanism of this transgene's destabilizing effect. Specifically, we find that this transgene shifts phenotype severity; however, the addition of the transgene does not just make all individuals maximally affected. In our most mild mutant allele, *mef2ca*^{b631}, phenotypes are not fully penetrant even in the presence of the transgene, suggesting that the transgene "tunes the dial" of severity. Previous work in yeast systems suggests that *Gal4* transgenes may have a squelching effect[37], and several researchers have suggested a negative impact of *Gal4* transgenes in zebrafish systems[31,38,39]. However, no one has demonstrated a mechanism for how *Gal4* impacts robustness in zebrafish. Based on the lack of overt phenotypes in wild types, zebrafish are likely robust to the impacts of this transgene, but lose their robustness in mutant systems.

Our findings challenge Waddington's canalization metaphor in that we discover that severe mutants consistently arrive in the same, new developmental canal. In each of our models, we find that the invariant phenotypes observed in severe mutants are not the result of a complete loss of a structure. For example, symplectic cartilage lengths are not all zero, and the opercle bone does not fail to form completely. Rather, a specific mutant phenotype becomes invariant. One could say that these mutants have been "neocanalized" into a new robust and repeatable developmental outcome. This formation of and fixation in a new canal could be analogous to the instability then stabilization that occurs in speciation events[40]. Could this be a similar series of events to what occurs when a new "wild-type" condition emerges in the founding of a new species? Although our neocanalized systems could not achieve fixation outside of a laboratory environment, we may be recapitulating a larger evolutionary phenomenon.

Methods

Zebrafish strains and husbandry

Zebrafish were maintained in accordance with established protocols[41,42]. All *mef2ca* alleles were maintained as heterozygotes by outcrossing to an AB background, which lost the natural sex

https://doi.org/10.1038/s41467-025-63316-2

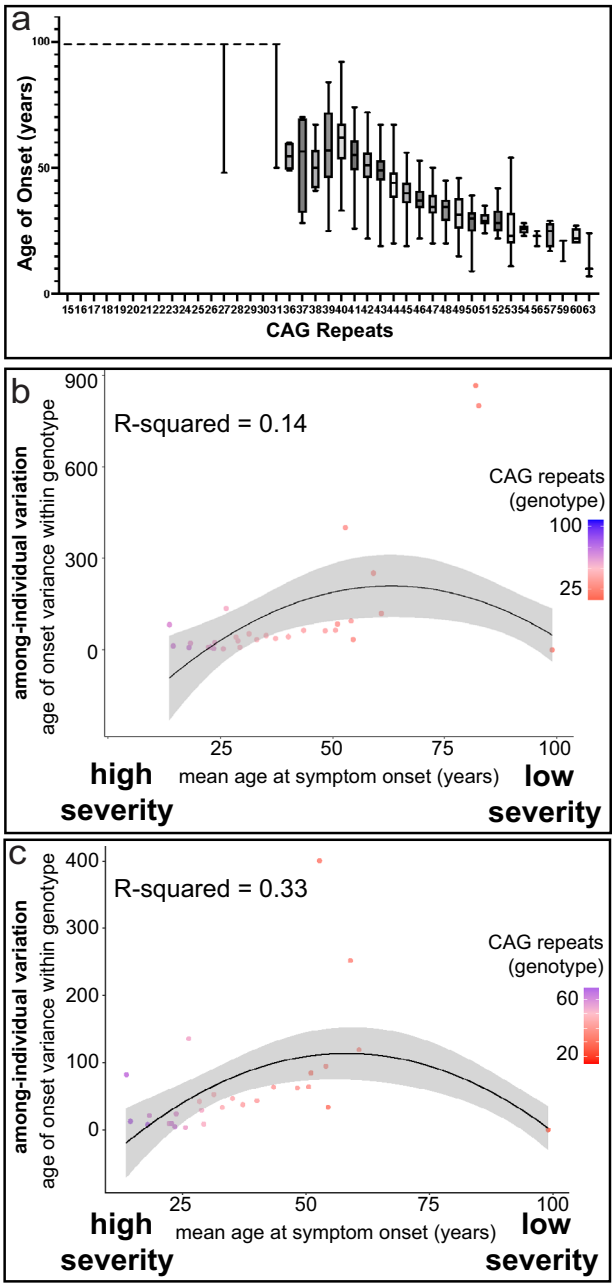

Fig. 5 | Huntington's disease demonstrates a quadratic relationship between severity and variation. a Huntington's disease genotypes CAG repeat number) are plotted against severity (age of onset). Significance bars are omitted for clarity; higher numbers of CAG repeats are associated with more severe disease. In box and whisker plot, the box covers the 25th to 75th quartiles, the line is at the median, and whiskers extend to the minimum and maximum values. **b** Each genotype was plotted by its age of onset as the *x*-coordinate and variance of age of onset as the *y*-coordinate. This represents among-individual variation. The R-squared for this relationship is indicated. **c** Outliers were removed from the dataset plotted in (**b**), and each genotype was plotted by its age of onset as the *x*-coordinate and variance of age of onset as the *y*-coordinate. This represents among-individual variation. The R-squared for this relationship is indicated. The gray bands in (**b**) and (**c**) represent 95% confidence intervals.

determinant[43]. We cannot determine the sex of any embryo or larva. All experiments are performed on both male and female animals without any knowledge of sex. The AB background we used is maintained as a closed colony in the University of Colorado zebrafish facility. The *fli1-F-hsp70l:Gal4VP16* transgene was maintained by outcrossing to the AB background, and these lines were maintained as heterozygotes to control Gal4 dosage. Wild types containing the *fli1:Gal4* transgene were outcrossed to heterozygotes for each *mef2ca* mutant allele. These animals were fluorescently sorted to identify transgene presence and confirmed to be heterozygous for the *mef2ca* allele by genotyping. All *fli1:Gal4* positive animals used in the described experiments were heterozygous. All of our work with zebrafish has been approved by the University of Colorado Institutional Animal Care and Use Committee (IACUC), Protocol #00188. All materials are freely available through the corresponding author.

CRISPR-Cas9 editing to produce *mef2ca*^{co3008} allele

CRISPR-Cas9 mutagenesis was employed following previously published protocols[44,45]. Briefly, sgRNAs were designed surrounding the coding region of *mef2ca*. The guides used to generate these mutants were: 5′-GGCTCCAAACTCTATATGGG-3′ and 5′-TCTCCTTCCTCTGTCGTTCC-3′. XbaI-digested pT3TS-nCas9n plasmid (Addgene plasmid #46757) was used as a template to transcribe Cas9 mRNA with the T3 mMESSAGE kit (Invitrogen). sgRNAs were transcribed from PCR-generated templates using the MEGAscript T7 Kit (Thermo Fisher Scientific). One-cell-stage embryos were injected with a mix of 200 ng/μl Cas9 mRNA and 50 ng/μl of each gene-specific sgRNA. Embryos were screened for the presence of a 241 bp PCR product that would only be produced in the case of a deletion with the following primers: Fw: 5′-ATTCTTAACCACGCCCCTTT-3′ Rv: 5′-TACAGTGAGCAGCGGAACGAGTG-3′.

Staining bone and cartilage for visualization

Six days post-fertilization, larvae were fixed and stained with Alcian Blue and Alizarin Red according to previously published protocols[33,46]. The craniofacial skeletons of these larvae were dissected and imaged with Nomarski imaging on a Leica DMi8 inverted microscope with a Leica DMC2900.

Phenotype scoring and symplectic cartilage measurement

After staining, each larva was genotyped with lysis of a piece of tail tissue, then scored for the presence or absence of six *mef2ca* mutant-associated phenotypes in line with methods previously published[5]. The penetrance score was calculated by scoring for the presence or absence of 12 phenotypes and counting how many phenotypes a given individual had. The phenotypes were: left side ectopic bone, right side ectopic bone, left jaw joint fused, right jaw joint fused, left symplectic shortened, right symplectic shortened, small Mc, obliterated Ch, small/reversed Ch, left hm joint fused, right hm joint fused, and ectopic cartilage. Symplectic cartilages were measured under a transmitted light dissecting scope, and images were taken with Zeiss ZEN software. A linear measurement was taken from the interhyal joint to the tip of the symplectic cartilage. This measurement was performed on the left and right sides, then the left and right sides were summed to get a total symplectic length for each animal. We calculated the absolute asymmetry, a combination of fluctuating and directional asymmetry, by determining the absolute value of the left minus the right side, or within-individual variation for each animal agnostic to side. We measured directional asymmetry by finding the mean difference between left and right sides for each genotype. To account for clutch-to-clutch differences in severity, at least three clutches per allele were scored and measured.

Genotyping assays

The *mef2ca*^{b1086} allele was genotyped using a KASP assay that has been previously described[33]. The *mef2ca*^{co3008} allele was genotyped using two PCR reactions per sample. One reaction detected the wild-type allele using the following primers: WT F: 5′-ATTCTTAACCACGCCCCTTT-3′ and WT R: 5′-TTCGTCCAAAATCATTTGACC-3′. This reaction yields a 378-base pair product. The other reaction detects the mutant allele with the

following primers: M F: TGGTTCATTCCGCACTTCAG and M R: AGGAAAGACTGCGCTGAGG. This reaction yields a 244 base pair product. Each reaction is run separately on a gel to determine the genotype of each larva. The *mef2ca*^{b631} allele is genotyped as previous[18] by RFLP (Restriction Fragment Length Polymorphism). The sequence of interest is amplified using the following primers: HOO_03: 5′-GGAAGGAGAAGGAGACGAGTGT-3′ and HOO_02: 5′-AATTACAAGTGCTTGATGTTTGGA-3′. This PCR yields a 361 base pair product, and to differentiate the presence of the mutation, the PCR product is digested with the BstNI restriction enzyme, yielding fragments of 290 and 71 base pairs in the mutant product and leaving the wild-type uncleaved.

Statistical analysis

A Fisher's exact test was used to calculate whether differences in phenotype penetrance were statistically significant. Statistical differences between total symplectic cartilage length, asymmetry, and average feature variances were calculated using Brown-Forsythe and Welch one-tailed ANOVA tests. Multiple comparisons were calculated and corrected for using a Dunnett T3 test. Cubic smoothing splines were used to estimate nonlinear trends in the relationships between symplectic length and variance, mean symplectic length and variance within a fish (left-right asymmetry), and age of onset of Huntington's disease by genotype severity. These were nonparametric exploratory plots. To estimate the trends seen in the spline plots using parametric methods, linear models with polynomials were used. Specifically, a quadratic trend was an appropriate fit for modeling symplectic length vs. variance. For each comparison, a linear model was used to estimate the quadratic relationship (1),

$$y \sim \beta_0 + \beta_l{}^{*}l + \beta_2{}^{*}l^2 + \epsilon$$

Where l represents symplectic length or mean symplectic, y represents variance of symplectic length, β represents regression coefficients, and ϵ represents random error. Total symplectic measurements represent distinct samples. For asymmetry, the left and right sides of the same animal were measured. For opercle measurements, the left and right sides were treated independently. For Huntington's analyses, there were 62 unique CAG values, but only 44 of these values had at least two observations to estimate standard deviation. Removing outliers with greater than 600 standard deviation resulted in 42 values in the final analyses.

Fluorescence imaging

Six days post-fertilization larvae were fixed and stained with Alcian Blue and Alizarin Red according to previously published protocols[33,46]. Larvae were mounted in 0.4% low-melt agarose for imaging. Fluorescent images of the Alizarin stain were captured on a Leica DMi8 microscope with an Andor Dragonfly 301 spinning disk confocal system, keeping all settings consistent across all samples.

Calculating area of opercle-branchiostegal ray complexes

The FIJI freehand selection tool was used to outline all bones in the opercle-branchiostegal ray (op-br) complexes and measure the area in pixels of each bone. Area was measured separately for the left and right side for each animal. Opercle and branchiostegal ray areas were summed if there were two separate bones.

Image-based profiling of opercle-branchiostegal ray complexes

Each z-stack of images was maximally projected into a 2D image. Images were then manually cropped to regions of interest containing the opercle and branchiostegal ray. From the cropped images, objects were segmented using Meta's segment anything model (SAM)[47]. After segmentation of opercle and branchiostegal ray bones, morphology features were extracted using CellProfiler[48]. The extracted image-based morphology features were cleaned, normalized, and feature selected using Cyto and pycytominer[34]. 269 of the 288 total extracted features were feature selected using variance thresholding. Variance thresholding removed features that have more than 5% of missing values across samples and/or features that have a ratio of 0.1 unique measurements compared to the number of samples. Variances of each feature were calculated and visualized on box and whisker plots.

Reporting summary

Further information on research design is available in the Nature Portfolio Reporting Summary linked to this article.

Data availability

All image analyses and image-based profiling can be found at: https://github.com/WayScience/Phenotypic_severity_and_variance. The CAG repeat data presented in the manuscript are based on the use of restricted study data, which can be requested from the dbGaP website under pht002988.v1.p1.c2. Excel file included in the manuscript. Source data are provided with this paper, including exact values and statistical analyses.

Code availability

All code is included in: https://github.com/WayScience/Phenotypic_severity_and_variance or https://zenodo.org/records/16747636[49] or available upon request.

References

1. Waddington, C. H. Canalization of development and the inheritance of acquired characters. *Nature* **150**, 563–565 (1942).
2. Hallgrímsson, B., Willmore, K. & Hall, BK. Canalization, developmental stability, and morphological integration in primate limbs. *Am. J. Phys. Anthropol.* **119**, 131–158 (2002).
3. Flatt, T. The evolutionary genetics of canalization. *Q. Rev. Biol.* **80**, 287–316 (2005).
4. Hallgrimsson, B. et al. The developmental-genetics of canalization. *Semin. Cell Dev. Biol.* **88**, 67–79 (2019).
5. Bailon-Zambrano, R. et al. Variable paralog expression underlies phenotype variation. *Elife* **11**, e79247 (2022).
6. Raj, A., Rifkin, S. A., Andersen, E. & van Oudenaarden, A. Variability in gene expression underlies incomplete penetrance. *Nature* **463**, 913–918 (2010).
7. Diss, G., Ascencio, D., DeLuna, A. & Landry, C. R. Molecular mechanisms of paralogous compensation and the robustness of cellular networks. *J. Exp. Zool. B Mol. Dev. Evol.* **322**, 488–499 (2014).
8. Vu, V. et al. Natural variation in gene expression modulates the severity of mutant phenotypes. *Cell* **162**, 391–402 (2015).
9. Queitsch, C., Sangster, T. A. & Lindquist, S. Hsp90 as a capacitor of phenotypic variation. *Nature* **417**, 618–624 (2002).
10. Rutherford, S. L. & Lindquist, S. Hsp90 as a capacitor for morphological evolution. *Nature* **396**, 336–342 (1998).
11. Green, R. M. et al. Developmental nonlinearity drives phenotypic robustness. *Nat. Commun.* **8**, 1970 (2017).
12. Fish, J. L. Developmental mechanisms underlying variation in craniofacial disease and evolution. *Dev. Biol.* **415**, 188–197 (2016).
13. Balasubramanian, M. et al. Case series: 2q33. 1 microdeletion syndrome—further delineation of the phenotype. *J. Med. Genet.* **48**, 290–298 (2011).
14. Hallgrímsson, B. et al. The brachymorph mouse and the developmental-genetic basis for canalization and morphological integration. *Evol. Dev.* **8**, 61–73 (2006).
15. Le Meur, N. et al. MEF2C haploinsufficiency caused by either microdeletion of the 5q14. 3 region or mutation is responsible for severe mental retardation with stereotypic movements, epilepsy and/or cerebral malformations. *J. Med. Genet.* **47**, 22–29 (2010).

16. Zweier, M. et al. Mutations in MEF2C from the 5q14. 3q15 microdeletion syndrome region are a frequent cause of severe mental retardation and diminish MECP2 and CDKL5 expression. *Hum. Mutat.* **31**, 722–733 (2010).
17. Tonk, V., Kyhm, J. H., Gibson, C. E. & Wilson, G. N. Interstitial deletion 5q14. 3q21. 3 with MEF2C haploinsufficiency and mild phenotype: when more is less. *Am. J. Med. Genet. A* **155**, 1437–1441 (2011).
18. Miller, C. T. et al. *mef2ca* is required in cranial neural crest to effect Endothelin1 signaling in zebrafish. *Dev. Biol.* **308**, 144–157 (2007).
19. Nichols, J. T. et al. Ligament versus bone cell identity in the zebrafish hyoid skeleton is regulated by mef2ca. *Development* **143**, 4430–4440 (2016).
20. Sucharov, J., Ray, K., Brooks, E. P. & Nichols, J. T. Selective breeding modifies mef2ca mutant incomplete penetrance by tuning the opposing Notch pathway. *PLoS Genet.* **15**, e1008507 (2019).
21. Van Valen, L. A study of fluctuating asymmetry. *Evolution* **16**, 125–142 (1962).
22. Palmer, A. R. & Strobeck, C. Fluctuating asymmetry: measurement, analysis, patterns. *Ann. Rev. Ecol. Syst.* **17**, 391–421 (1986).
23. Klingenberg, C. P. A developmental perspective on developmental instability: theory, models and mechanisms in *Developmental Instability: Causes and Consequences*, 14–34 (Oxford University Press, 2003).
24. Polak, M. *Developmental Instability: Causes and Consequences* (Oxford University Press, 2003).
25. Palmer, A. R. & Strobeck, C. Fluctuating asymmetry as a measure of developmental stability: implications of non-normal distributions and power of statistical tests. *Acta Zool. Fennica* **191**, 13 (1992).
26. Palmer, A. R. & Strobeck, C. Fluctuating asymmetry analyses revisited in *Developmental Instability: Causes and Consequences*, 279–319 (Oxford University Press, 2003).
27. Palmer, A. R. Fluctuating asymmetry analyses: a primer in *Developmental Instability: Its Origins and Evolutionary Implications* (Springer, 1994).
28. Graham, J. H., Raz, S., Hel-Or, H. & Nevo, E. Fluctuating asymmetry: methods, theory, and applications. *Symmetry* **2**, 466–540 (2010).
29. DeLaurier, A. et al. Role of *mef2ca* in developmental buffering of the zebrafish larval hyoid dermal skeleton. *Dev. Biol.* **385**, 189–199 (2014).
30. Kimmel, C. B. et al. Transgene-mediated skeletal phenotypic variation in zebrafish. *J. Fish. Biol.* **98**, 956–970 (2021).
31. Köster, R. W. & Fraser, S. E. Tracing transgene expression in living zebrafish embryos. *Dev. Biol.* **233**, 329–346 (2001).
32. Fisher, R. A. XV.—The correlation between relatives on the supposition of Mendelian inheritance. *Earth Environ. Sci. Trans. R. Soc. Edinb.* **52**, 399–433 (1919).
33. Brooks, E. & Nichols, J. Shifting zebrafish lethal skeletal mutant penetrance by progeny testing. *J. Vis. Exp.* **1**, 56200 (2017).
34. Serrano, E. et al. Reproducible image-based profiling with Pycytominer. *Nat. Methods* **22**, 677–680 (2024).
35. Lee, J.-M. et al. CAG repeat expansion in Huntington disease determines age at onset in a fully dominant fashion. *Neurology* **78**, 690–695 (2012).
36. Keum, J. W. et al. The HTT CAG-expansion mutation determines age at death but not disease duration in Huntington disease. *Am. J. Hum. Genet.* **98**, 287–298 (2016).
37. Gill, G. & Ptashne, M. Negative effect of the transcriptional activator GAL4. *Nature* **334**, 721–724 (1988).
38. Asakawa, K. et al. Genetic dissection of neural circuits by Tol2 transposon-mediated Gal4 gene and enhancer trapping in zebrafish. *Proc. Natl. Acad. Sci. USA* **105**, 1255–1260 (2008).
39. Scott, E. K. et al. Targeting neural circuitry in zebrafish using GAL4 enhancer trapping. *Nat. Methods* **4**, 323–326 (2007).
40. Lamichhaney, S. et al. Rapid hybrid speciation in Darwin's finches. *Science* **359**, 224–228 (2018).
41. Westerfield, M. *The Zebrafish Book: A Guide for the Laboratory Use of Zebrafish (Brachydanio rerio)* (University of Oregon Press, Eugene, 1993).
42. Kimmel, C. B., Ballard, W. W., Kimmel, S. R., Ullmann, B. & Schilling, T. F. Stages of embryonic development of the zebrafish. *Dev. Dyn.* **203**, 253–310 (1995).
43. Wilson, C. A. et al. Wild sex in zebrafish: loss of the natural sex determinant in domesticated strains. *Genetics* **198**, 1291–1308 (2014).
44. Hwang, W. Y. et al. Efficient genome editing in zebrafish using a CRISPR-Cas system. *Nat. Biotechnol.* **31**, 227–229 (2013).
45. Mitchell, J. M. et al. The alx3 gene shapes the zebrafish neurocranium by regulating frontonasal neural crest cell differentiation timing. *Development* **148**, dev197483 (2021).
46. Walker, M. B. & Kimmel, C. B. A two-color acid-free cartilage and bone stain for zebrafish larvae. *Biotech. Histochem.* **82**, 23–28 (2007).
47. Kirillov, A. et al. Segment anything. In *Proc. IEEE/CVF International Conference on Computer Vision*, 3992–4003 (2023).
48. Stirling, D. R. et al. CellProfiler 4: improvements in speed, utility and usability. *BMC Bioinform.* **22**, 1–11 (2021).
49. Lippincott, M. et al. WayScience/Phenotypic_severity_and_variance: v01. Zenodo https://doi.org/10.5281/zenodo.16747636 (2025).

Acknowledgements

We would like to thank Chuck Kimmel, Jeff Moore, and members of the Nichols Laboratory and the Department of Craniofacial Biology for their thoughtful comments. We would like to thank Jenna Tomkinson, Dave Bunten, and Erik Serrano for performing code review on the image-based profiling pipeline and analyses. This work was funded by the National Institutes of Health (R01DE029193 to J.T.N.) and National Science Foundation (GRFP 1938058 to A.M.M. and GRFP 2439026 to G.E.G.).

Author contributions

Conceptualization: A.M.M., J.T.N.; Methodology: A.M.M., R.B.Z., C.A.H., J.S., G.E.G., M.J.L., K.L.C., J.T.N.; Software: N/A; Validation: J.T.N.; Formal analysis: A.M.M., G.P.W., K.A.C., J.T.N.; Investigation: A.M.M., J.T.N.; Data curation: A.M.M., J.T.N.; Writing—original draft: A.M.M., J.T.N.; Writing—review & editing: A.M.M., G.E.G., J.T.N.; Visualization: A.M.M., K.L.C., J.T.N.; Supervision: J.T.N.; Project administration: J.T.N.; Funding acquisition: J.T.N.

Competing interests

The authors declare no competing interests.

Additional information

Supplementary information The online version contains supplementary material available at https://doi.org/10.1038/s41467-025-63316-2.

Correspondence and requests for materials should be addressed to James T. Nichols.

Peer review information *Nature Communications* thanks Rebecca Green and the other anonymous reviewer(s) for their contribution to the peer review of this work. A peer review file is available.